

# High-Resolution Spectroscopy of Gamma-Ray Lines from the X-Class Solar Flare of 23 July, 2002

D. M. Smith<sup>1</sup>, G. H. Share<sup>2</sup>, R. J. Murphy<sup>2</sup>, R. A. Schwartz<sup>3,4</sup>, A. Y. Shih<sup>1,5</sup>, R. P. Lin<sup>1,5</sup>

## ABSTRACT

The *Reuven Ramaty High Energy Solar Spectroscopy Imager (RHESSI)* has obtained the first high-resolution measurements of nuclear de-excitation lines produced by energetic ions accelerated in a solar flare, a GOES X4.8 event occurring on 23 July, 2002 at a heliocentric angle of  $\sim 73^\circ$ . Lines of neon, magnesium, silicon, iron, carbon, and oxygen were resolved for the first time. They exhibit Doppler redshifts of 0.1–0.8% and broadening of 0.1–2.1% (FWHM), generally decreasing with mass. The measured redshifts are larger than expected for a model of an interacting ion distribution isotropic in the downward hemisphere in a radial magnetic field. Possible interpretations of the large redshifts include 1) an inclination of the loop magnetic field to the solar surface so that the ion distribution is oriented more directly away from the observer, and 2) extreme beaming of the ions downward along a magnetic field normal to the solar surface. Bulk downward motion of the plasma in which the accelerated ions interact can be ruled out.

*Subject headings:* Sun:flares — Sun:X-rays, gamma rays — line:profiles — gamma rays:observations

## 1. Introduction

We report the first high-energy-resolution measurements of nuclear de-excitation lines in a solar flare. These lines were detected by the *Reuven Ramaty High Energy Solar Spectroscopic Imager (RHESSI)* during the GOES X4.8-class solar flare of 23 July, 2002, which

---

<sup>1</sup>Space Sciences Laboratory, University of California, Berkeley, Berkeley, CA 94720

<sup>2</sup>E. O. Hulbert Center for Space Research, Naval Research Laboratory, Washington, DC 20375

<sup>3</sup>NASA Goddard Space Flight Center, Greenbelt, MD, 20771

<sup>4</sup>Science Systems & Applications, Inc.

<sup>5</sup>Department of Physics, University of California, Berkeley, Berkeley, CA 94720

occurred at coordinates S13E72 on the solar disk ( $73^\circ$  heliocentric angle). The characteristics of this flare are reviewed in depth in Lin et al. (2003).

Gamma-ray lines from inelastic interactions of accelerated ions with ambient nuclei in solar flares (Lingenfelter & Ramaty 1967) were first observed by Chupp et al. (1973). The de-excitation lines can be Doppler shifted due to the nuclear recoils from the ion interaction and the emission of the gamma ray. The line profiles thus reveal the angular distribution of the interacting ions (Ramaty and Crannell 1976). Accelerated protons and  $\alpha$ -particles produce narrow lines while accelerated heavy ions produce broad lines which merge together to form an underlying nuclear continuum. Share et al. (2002) analyzed an ensemble of gamma-ray line flares from the *Solar Maximum Mission* Gamma-Ray Spectrometer (*SMM/GRS*). They found that narrow lines exhibit  $\sim 1\%$  redshift for flares at small heliocentric angles, but are not appreciably shifted near the limb of the Sun. Their measurements are consistent with a distribution of interacting particles which is isotropic in the downward hemisphere and zero in the upward hemisphere.

Although the *SMM/GRS* data yielded useful measurements of some nuclear-line redshifts and put constraints on the line widths, the energy resolution of that instrument was moderate, averaging around 4% FWHM over the nuclear-line range. *RHESSI* (Lin et al. 2002) was designed to provide high-resolution measurements of the shape and redshift of de-excitation lines using cryogenically cooled germanium detectors to achieve an energy resolution averaging around 0.2% FWHM from 1–6 MeV (Smith et al. 2002).

## 2. Analysis and Results

The *RHESSI* spectrometer consists of nine coaxial germanium detectors, each divided into a  $\sim 1$  cm upper segment (which stops most hard x-rays) and a  $\sim 7$  cm rear segment. Here we use only data from the rear segments, which have most of the efficiency for stopping gamma-rays above 300 keV (Smith et al. 2002). Detector #2, which is operated in an unsegmented mode and has degraded energy resolution, was not used. The spectra in Figure 1 were accumulated from 00:27:20 to 00:43:20 UT on 23 July, 2002, an interval that includes most of the high-energy emission from this flare (Lin et al. 2003).

The flare intensity is roughly half the background level above  $\sim 1$  MeV. The instrumental gamma-ray background is caused by the interactions of cosmic rays and protons trapped in the radiation belts with materials in the spacecraft and the atmosphere. Every 15 orbits (about one day), the geomagnetic coordinates of the spacecraft approximately repeat themselves, and therefore so do the cosmic and trapped particle fluxes. Thus we model the

background during the flare with the average of two spectra, taken 15 orbits before and after the flare, each of which is the same length as the flare observation itself. Above 3 MeV, however, we replaced this background spectrum with a different one using a full day’s integrated data. In this high-energy band the background is simple in form and nearly free of lines, so that we can get an accurate background estimate with small statistical fluctuations, regardless of the exact orbital parameters, simply by rescaling the full-day integration to match the intensity of the  $\pm 15$ -orbit spectrum.

The full spectrum (shown in Lin et al. (2003)) from 250 keV to 8.5 MeV was fitted with six bright de-excitation lines (Table 1) plus a broken power-law representing electron bremsstrahlung (the index hardens from 2.77 to 2.23 at a break energy of 617 keV). It was also necessary to represent two other components of the spectrum: the very broad lines from interactions of accelerated heavy ions with ambient hydrogen, and the faint lines from other proton- and  $\alpha$ -induced lines that cannot be measured individually. Within the statistical limitations of the data, the sum of these components is well-represented by three very broad Gaussians centered at 1845, 4358 and 6575 keV. Bright narrow lines were included from positron annihilation (Share et al. 2003a) and neutron capture (Murphy et al. 2003) at 511 keV and 2223 keV, respectively. Finally, weak lines at 1263 keV and 6918 keV of intermediate width were also included, representing expected features which are compounds of more than one line.

The fitting was done with the Spectral Executive (SPEX) package (Schwartz 1996), taking into account the full diagonal and off-diagonal response of the instrument (Smith et al. 2002). The spectra for the six bright de-excitation lines are shown in Figure 1 and the fit parameters are given in Table 1. The features at  $\sim 840$  keV in the upper left panel of Figure 1 and  $\sim 1807$  keV in the lower left panel may be the 844 keV and 1809 keV solar de-excitation lines of aluminum (Kozlovsky, Murphy & Ramaty 2002), but if so are at a surprisingly high flux. The effect of the instrumental resolution (about 3.0 keV at 847 keV, 4.1 keV at 1779 keV, and  $\sim 10$  keV at 6129 keV) has been removed from the width measurements, but, except for the  $^{56}\text{Fe}$  line, it is negligible compared to the solar line widths. The best-fit Gaussians and their zero-redshift versions are also shown in Figure 1. Zero redshift is visibly inconsistent with the data for most lines.

The redshifts and widths from Table 1 are shown in Figure 2. Heavier nuclei will recoil less from a collision with a proton or  $\alpha$ -particle, and will thus show less redshift and broadening. This trend is clearly visible. The expected relation is not exactly linear, since the average energy of the accelerated particles interacting with each nucleus depends on the the cross section for excitation. The neon line, which appears to have a redshift below the trend in Figure 2, has the lowest threshold for excitation.

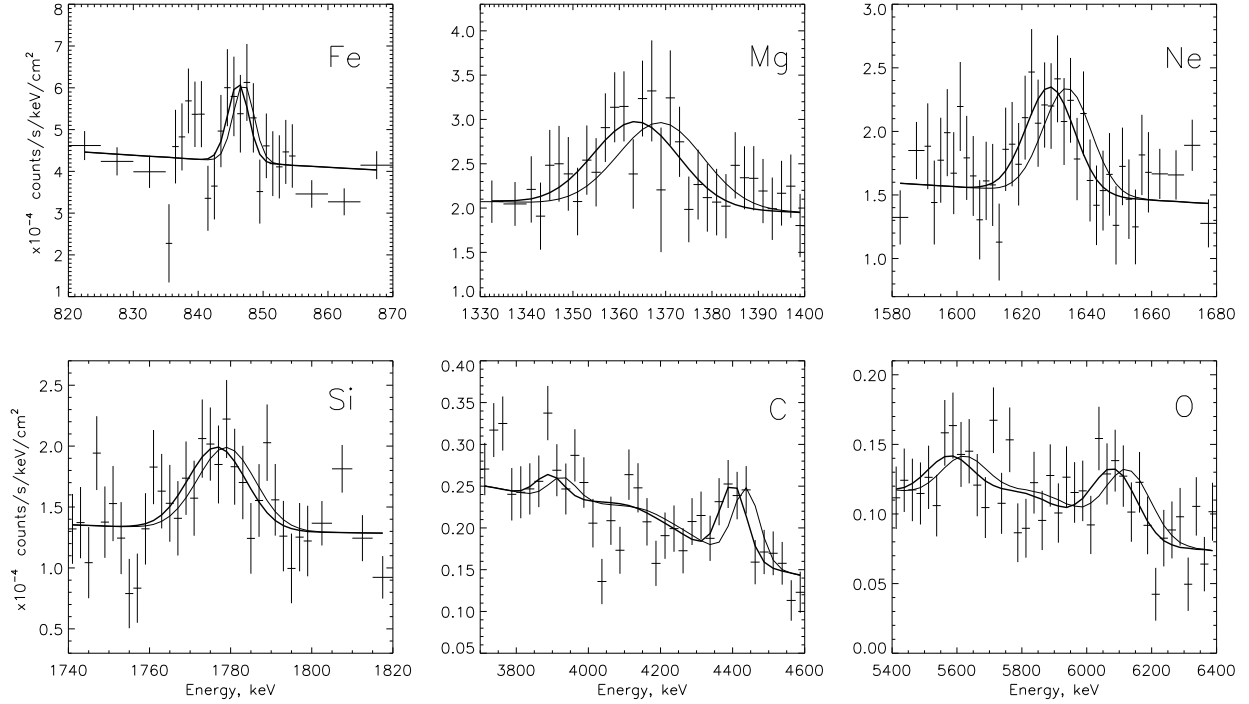


Fig. 1.— *RHESSI* background-subtracted count spectra from 00:27:20 UT to 00:43:20 UT on 23 July, 2002. Each panel is labeled with the element primarily responsible for the line shown. The carbon and oxygen lines also show the secondary peak from escape of a 511 keV positron-annihilation photon, which also contains information on the line shape. The heavy curve shown in each panel is the Gaussian fit from Table 1 plus the underlying bremsstrahlung continuum and broad lines (see text), convolved with the instrument response. The lighter line is the same fit forced to zero redshift for comparison. The error bars are  $\pm 1\sigma$  from Poisson statistics.

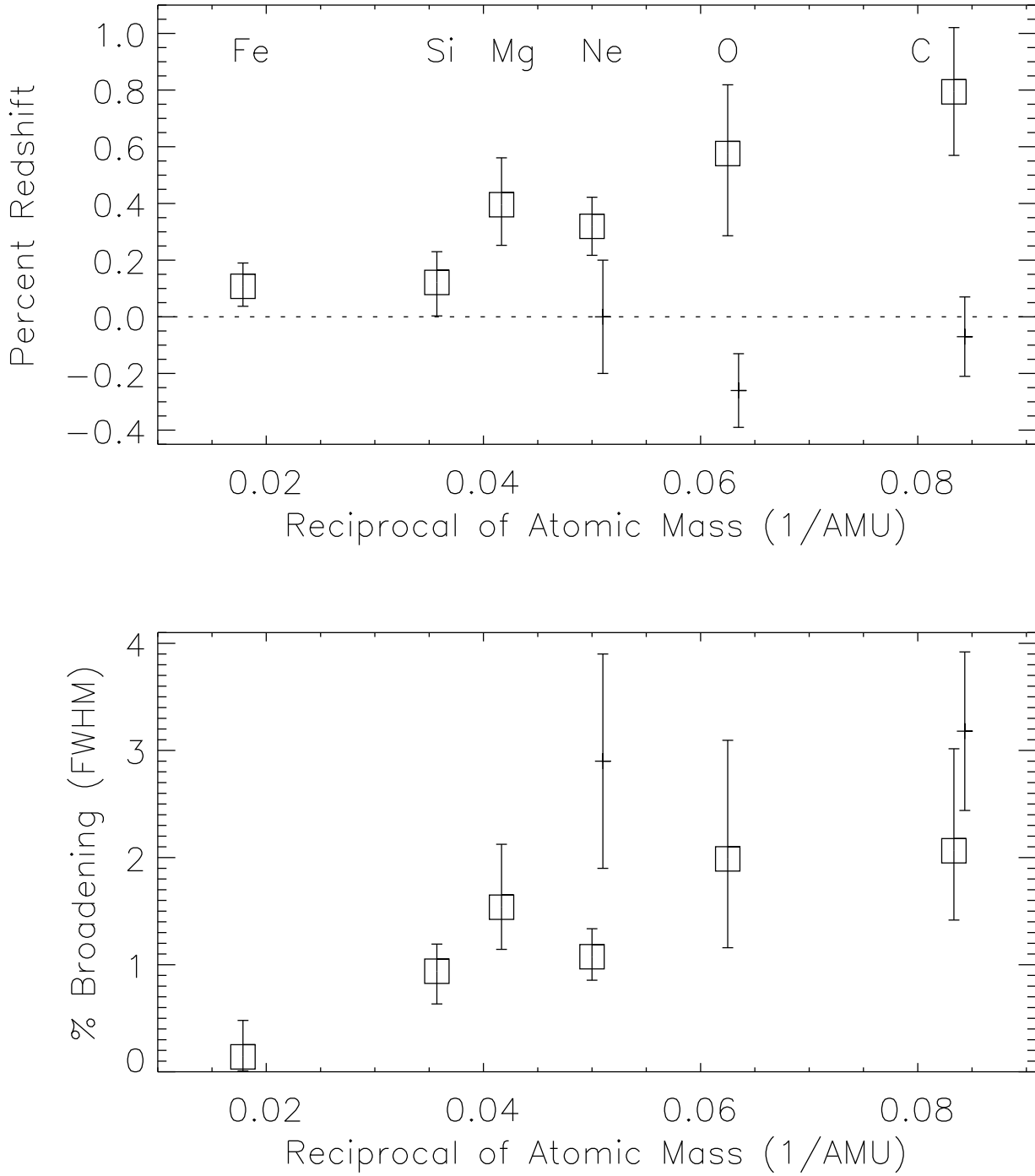


Fig. 2.— Redshift (top) and Doppler broadening (bottom) from Table 1 plotted as a function of the reciprocal of the mass of the nucleus. Data points marked as squares are from this flare. Data points marked with dashes are the average of five flares observed by *SMM*/GRS near  $74^\circ$  heliocentric angle.

### 3. Discussion

The sum of the fluences in the narrow lines of Table 1 is  $137 \text{ ph cm}^{-2}$ . Share & Murphy (1995) calculated the total fluence in narrow lines for 19 X-class flares observed by *SMM*/GRS. Estimating the contribution of fainter lines not in Table 1 by comparison with the flares studied by Share & Murphy (1995) gives a total line fluence of about  $180 \text{ ph cm}^{-2}$  for this flare, similar to the brighter events from *SMM*/GRS, which include flares from GOES class X2.8 to X15.0.

Table 1 and Figure 2 also show *SMM*/GRS results from Share et al. (2002) for the average of five flares close to a heliocentric angle of  $74^\circ$ . The most striking difference is the lack of redshift in the lines from carbon and oxygen, in significant disagreement with our result for the 23 July 2002 flare. The null redshift and high broadening in the *SMM*/GRS neon line are in marginal disagreement with *RHESSI* as well. The advantage of high energy resolution is clear: the *RHESSI* results are more precise using a single flare than the *SMM*/GRS result for the average of five flares, even though *RHESSI* is a smaller instrument. With more flares observed at high resolution, we will be able to tell whether this disagreement between *RHESSI* and *SMM*/GRS is due to intrinsic variations between flares or to the limitations of *SMM*'s moderate-resolution spectroscopy.

We use the modeling code of Murphy, Kozlovsky & Ramaty (1988), which allows an arbitrary angular distribution of interacting particles about an axis at an arbitrary angle to the observer ( $\theta$ ). For particles distributed with respect to a radial field line,  $\theta$  is equal to the heliocentric angle,  $73^\circ$  for this flare. The simulation generates separate gamma-ray spectra for  $\alpha$ -particles and protons, and includes the effects of nuclear recoil both from the interaction and the emission of the gamma ray. Thus, even a purely downward beam of incident protons gives broadened lines due to the range of recoil angles.

We simulated two angular distributions for the interacting ions: 1) isotropic within the forward hemisphere and zero in the hemisphere toward the observer, and 2) beamed directly forwards. Since we will explore the possibility that the magnetic field is not perpendicular to the solar surface, we will use “forward” to mean along the magnetic field away from the observer and “downward” to mean perpendicular to the solar surface.

Distributions with no forward bias, such as a fan beam or a full isotropic distribution, give no redshift and thus disagree strongly with the redshift values in Table 1. For each of the distributions, the viewing angle  $\theta$  was run at  $0^\circ$ ,  $30^\circ$ ,  $45^\circ$ ,  $52^\circ$ ,  $60^\circ$ , and  $73^\circ$ . Interpolations along  $\cos(\theta)$  gave line shapes for intermediate angles. The proton and  $\alpha$ -particle energy spectra were modeled as power laws with index  $-3.75$ , and the  $\alpha$ /proton ratio was fixed at 0.5, both consistent with results from *SMM*/GRS (Share & Murphy 1995, 1998). Figure 3

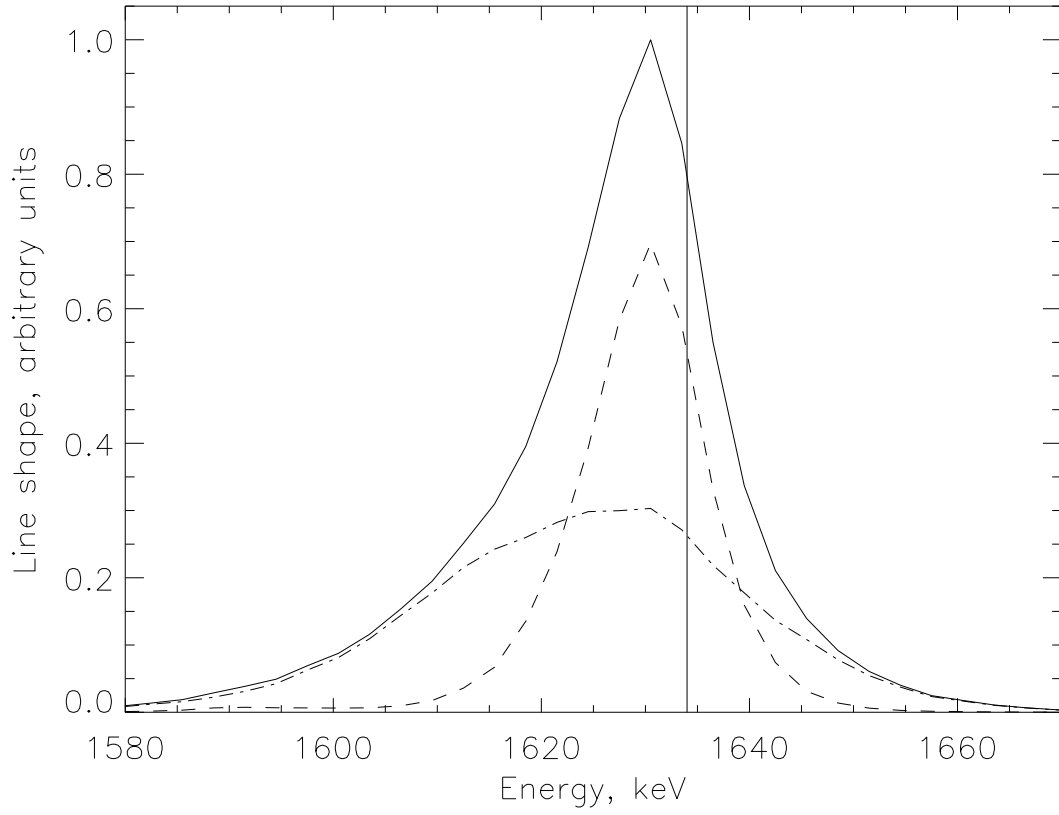


Fig. 3.— Model  $^{20}\text{Ne}$  line shape for a power-law index of  $-3.75$ , a viewing angle of  $30^\circ$ , and a forward-isotropic distribution. Dashed line: line shape from interacting protons. Dash-dotted line: line shape from interacting  $\alpha$ -particles. Solid curve: total line shape for an  $\alpha$ /proton ratio of  $0.5$ . Vertical line: the rest energy of the de-excitation line,  $1634$  keV.

shows the  $^{20}\text{Ne}$  line shape predicted by the forward-isotropic model for a viewing angle of  $30^\circ$ .

For both models and each viewing angle, we fitted the model lineshapes (e.g. Figure 3) to the data, allowing the line fluences and the underlying broad lines and continuum to vary to minimize  $\chi^2$ . Figure 4 shows the relative  $\chi^2$  for the two angular distributions and all viewing angles. The forward isotropic model is clearly a much better fit, but it fits best with a viewing angle of  $30\text{--}40^\circ$ . If the field lines of the loop were perpendicular to the solar surface at their base, where the ions interact, the viewing angle would be the heliocentric angle of the flare,  $73^\circ$ . This is inconsistent with the data at greater than 99% confidence. *RHESSI's* ability to image gamma rays allows us to be certain that the line emission comes from near the flare, i.e. near  $73^\circ$  (Hurford et al. 2003).

We have run further simulations with power-law indices from  $-1.75$  to  $-4.75$  and  $\alpha$ /proton ratios from 0.0 to 2.5. In all cases the best-fit viewing angle for the forward isotropic case is close to  $30\text{--}40^\circ$  and inconsistent with  $73^\circ$ . Note that even the forward beam, which produces the maximum possible redshift of any distribution, still fits best with a viewing angle smaller than the heliocentric angle. For spectral index  $-2.75$  and harder, the forward beam can fit as well as the forward isotropic distribution.

A redshift could be caused either by recoil from an anisotropic distribution of interacting ions or by bulk motion away from the observer of the medium in which they interact. We believe the latter is not significant here for two reasons. First, in the case of bulk motion the percentage redshift is a constant, and not inversely proportional to the mass of the excited nucleus (Figure 2). Second, although downward flows in the chromosphere have been observed in impulsive flare events via red wings in  $\text{H}\alpha$  line profiles, the velocities are only  $20\text{--}50$  km/s (e.g. Wülser, Canfield & Zarro 1992), implying redshifts of no more than  $0.007\text{--}0.017\%$ , a trivial fraction of the total gamma-ray shifts.

Two explanations remain for the large redshifts: either the field lines in the loop legs are inclined toward us instead of being perpendicular to the solar surface, or else the angular distribution of the interacting particles is closer to a pure forward beam than a forward-isotropic distribution. Forward-isotropic or isotropic distributions of interacting  $\alpha$ -particles are strongly favored over a downward beam in a study of the lines at  $0.429$  and  $0.478$  MeV from  $\alpha\text{--}\alpha$  reactions in this flare (Share et al. 2003b) and in flares observed with *SMM/GRS* (Share & Murphy 1997). Also, the low average redshifts of the  $^{20}\text{Ne}$ ,  $^{12}\text{C}$  and  $^{16}\text{O}$  lines in all the flares seen by *SMM/GRS* (Share et al. 2002), including those used in Table 1, favored a downward isotropic distribution (or one with a slight additional upward component) to a downward beam.



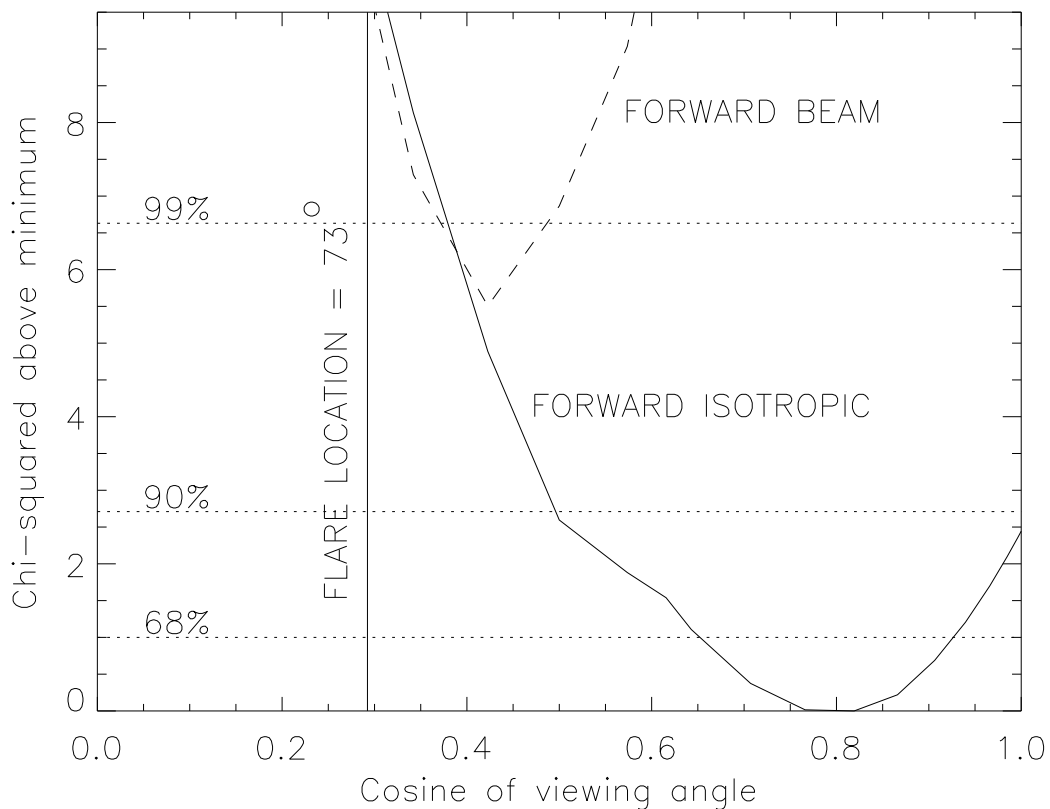


Fig. 4.— Relative values of  $\chi^2$  for model fits to the 23 July flare data at various viewing angles. Solid curve: forward-isotropic distribution. Dashed curve: forward beam. Dotted lines: confidence levels for the hypothesis that the best fit is preferred to a given model. The left edge of the plot corresponds to a loop viewed side-on, the right edge to a loop viewed down along the legs, and the vertical line corresponds to a loop perpendicular to the local solar surface.

If, on the other hand, magnetic loops containing accelerated ions are inclined from the perpendicular for this flare, it may help explain why the *SMM*/GRS widths are larger than ours in Table 1. Share et al. (2002) combined five flares to get their result near  $74^\circ$ , and if these had a wider range of  $\theta$  than of heliocentric angle, differing redshifts could combine to make a broader line. Solar active regions often do contain inclined loops, and the magnetic topology of regions such as this one (“ $\beta\gamma\delta$ ”) that produce the largest flares also tend to be the most complex.

A more detailed analysis of nuclear de-excitation line shapes can constrain not only the angular distribution of the particles but also the  $\alpha$ /proton ratio (as can be seen from the different component shapes in Figure 3) and even the spectral index. The full power of the spectral analysis of gamma-ray lines, however, will be realized when the constraints imposed by the line shapes are combined with information from the gamma-ray line fluences and from other observations such as gamma-ray and x-ray imaging (Hurford et al. 2003), magnetograms and imaging at other wavelengths, and the decay profile of the neutron-capture line (Murphy et al. 2003).

The work at the University of California, Berkeley and at NASA’s Goddard Space Flight Center was supported by NASA contract NAS5-98033, and that at the Naval Research Laboratory by NASA DPR W19746. We thank Hugh Hudson, Gordon Hurford, Brian Dennis, George Fisher, and Benzion Kozlovsky for useful discussions.

## REFERENCES

- Chupp, E. L., Forrest, D. J., Higbie, P. R., Suri, A. N., Tsai, C., & Dunphy, P. P. 1973, *Nature*, 241, 333
- Hurford, G. J., Schwartz, R. A., Krucker, S., Lin, R. P., Smith, D. M. & Vilmer, N. 2003, *ApJ*, this issue
- Kozlovsky, B., Murphy, R. J., & Ramaty, R. 2002, *ApJ*, 141, 523
- Lin, R. P. et al. 2002, *Solar Physics*, 210, 3
- Lin, R. P. et al. 2003, *ApJ*, this issue
- Lingenfelter, R. E. & Ramaty, R. 1967, in *High Energy Nuclear Reactions in Astrophysics*, ed. B. S. P. Shen (New York: W. A. Benjamin), p. 99.
- Murphy, R. J., Kozlovsky, B., & Ramaty R. 1988, *ApJ*, 331, 1029

- Murphy, R. J., Share, G. H., Hua, X.-M., Lin, R. P., Smith, D. M., & Schwartz, R. A. 2003, ApJ, this issue
- Ramaty, R. and Crannell, C. J. 1976, ApJ, 203, 766
- Schwartz, R. A. 1996, “Compton Gamma Ray Observatory Phase 4 Guest Investigator Program: Solar Flare Hard X-ray Spectroscopy,” Technical Report, NASA Goddard Space Flight Center
- Share, G. H. & Murphy, R. J. 1995, ApJ, 452, 933
- Share, G. H. & Murphy, R. J. 1997, ApJ, 485, 409
- Share, G. H. & Murphy, R. J. 1998, ApJ, 508, 876
- Share, G. H., Murphy, R. J., Kiener, J., & de Séréville, N. 2002, ApJ, 573, 464
- Share, G. H., Murphy, R. J., Smith, D. M., Lin, R. P., Dennis, B. R., & Schwartz, R. A. 2003b, ApJ, this issue
- Share, G. H., Smith, D. M., Lin, R. P., Shih, A. Y., Hudson, H., Schwartz, R. A., Kozlovsky, B., & Skibo, J. G. 2003a, ApJ, this issue
- Smith, D. M. et al. 2002, Solar Physics, 210, 33
- Wülser, J.-P., Canfield, R. C., & Zarro, D. M. 1992, ApJ, 384, 341

Table 1. Best fit Gaussian parameters for prompt nuclear lines

Isotope	Rest Energy (keV)	Fit Energy (keV)	% Redshift	FWHM (keV)	% FWHM	Fluence (ph cm <sup>-2</sup> )	<i>SMM</i> / <i>GRS</i> % Redshift <sup>a</sup>	<i>SMM</i> / <i>GRS</i> % FWHM <sup>a</sup>
<sup>56</sup> Fe	847	846.09 <sup>+0.70</sup> <sub>-0.60</sub>	0.11 <sup>+0.08</sup> <sub>-0.07</sub>	1.2 <sup>+2.9</sup> <sub>-1.1</sub>	0.14 <sup>+0.34</sup> <sub>-0.13</sub>	7.5 <sup>+3.4</sup> <sub>-2.3</sub>	...	...
<sup>24</sup> Mg	1369	1363.6 <sup>+2.3</sup> <sub>-2.0</sub>	0.40 <sup>+0.17</sup> <sub>-0.14</sub>	21.0 <sup>+8.0</sup> <sub>-5.4</sub>	1.54 <sup>+0.59</sup> <sub>-0.39</sub>	28.3 <sup>+7.2</sup> <sub>-6.6</sub>	...	...
<sup>20</sup> Ne	1634	1628.8 <sup>+1.7</sup> <sub>-1.7</sub>	0.32 <sup>+0.10</sup> <sub>-0.10</sub>	17.6 <sup>+4.3</sup> <sub>-3.6</sub>	1.07 <sup>+0.26</sup> <sub>-0.22</sub>	21.4 <sup>+3.8</sup> <sub>-4.5</sub>	0.0 ± 0.2	2.9 ± 1.0
<sup>28</sup> Si	1779	1776.8 <sup>+1.9</sup> <sub>-2.1</sub>	0.12 <sup>+0.11</sup> <sub>-0.12</sub>	16.7 <sup>+4.5</sup> <sub>-5.4</sub>	0.94 <sup>+0.25</sup> <sub>-0.30</sub>	17.1 <sup>+4.0</sup> <sub>-4.5</sub>	...	...
<sup>12</sup> C	4438	4403 <sup>+10</sup> <sub>-10</sub>	0.79 <sup>+0.23</sup> <sub>-0.22</sub>	92 <sup>+42</sup> <sub>-29</sub>	2.06 <sup>+0.95</sup> <sub>-0.65</sub>	28.6 <sup>+13.1</sup> <sub>-8.6</sub>	-0.07 ± 0.14 <sup>b</sup>	3.18 ± 0.74
<sup>16</sup> O	6129	6094 <sup>+15</sup> <sub>-18</sub>	0.58 <sup>+0.24</sup> <sub>-0.29</sub>	122 <sup>+68</sup> <sub>-51</sub>	1.99 <sup>+1.11</sup> <sub>-0.83</sub>	34.2 <sup>+12.8</sup> <sub>-15.5</sub>	-0.26 ± 0.13 <sup>b</sup>	...

<sup>a</sup>Average of five flares near heliocentric angle 74°

<sup>b</sup>Blueshift